AD-A158 171 BOUNDARY INTEGRAL TECHNIQUES FOR MULTI-CONNECTED DOMAINS(U) WISCONSIN UNIV-MADISON MATHEMATICS RESEARCH CENTER G R BAKER ET AL. JUN 85 MRC-TSR-2830 1/1

UNCLASSIFIED DAAG29-80-C-0041 F/G 12/1 NL

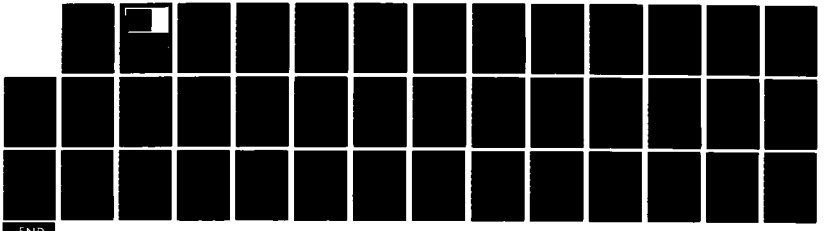

END

FILMED

DTIC

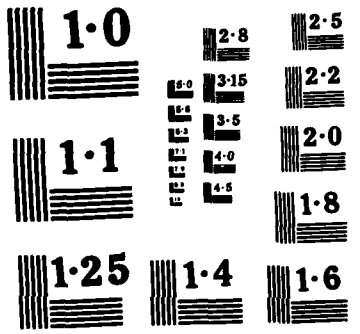

NATIONAL BUREAU OF STANDARDS
MICROCOPY RESOLUTION TEST CHART

MRC Technical Summary Report #2830

BOUNDARY INTEGRAL TECHNIQUES FOR MULTI-CONNECTED DOMAINS

G. R. Baker and M. J. Shelley

Mathematics Research Center
University of Wisconsin—Madison
610 Walnut Street
Madison, Wisconsin 53705

June 1985

(Received March 11, 1985)

Approved for public release
Distribution unlimited

Sponsored by

U. S. Army Research Office
P. O. Box 12211
Research Triangle Park
North Carolina 27709

National Aeronautics & Space Administration
Washington, DC 20546

National Science Foundation
Washington, DC 20550

UNIVERSITY OF WISCONSIN-MADISON
MATHEMATICS RESEARCH CENTER

BOUNDARY INTEGRAL TECHNIQUES FOR MULTI-CONNECTED DOMAINS

G. R. Baker* and M. J. Shelley*

Technical Summary Report #2830
June 1985

ABSTRACT

Several boundary integral techniques are available for the computation of the solution to Laplace's equation in multi-connected domains. However, for cases where the domain is changing, such as in incompressible, inviscid fluid flow with free surfaces, iterative methods are highly attractive. The paper describes one such formulation and tests it on circular and elliptic annuli. It is necessary to use interpolated quadrature points to maintain accuracy when regions of the annuli are thin.

AMS (MOS) Subject Classifications: 65N99, 65R20, 76B15

Key Words: Boundary integral techniques, multi-connected domains, Fredholm integral equations

Work Unit Number 2 (Physical Mathematics)

*Department of Mathematics, University of Arizona, Tucson, Arizona 85710

Partially sponsored by the United States Army under Contract No. DAAG29-80-C-0041, the National Science Foundation, Grant No. MCS-8302549, and by NASA, Grant No. NGT 03002800.

SIGNIFICANCE AND EXPLANATION

Several boundary integral techniques are available for the computation of the solution to Laplace's equation in multi-connected domains. However, for cases where the domain is changing, such as in incompressible, inviscid fluid flow with free surfaces, iterative methods are highly attractive. The paper describes one such formulation and tests it on circular and elliptic annuli. It is necessary to use interpolated quadrature points to maintain accuracy when regions of the annuli are thin.

BOUNDARY INTEGRAL TECHNIQUES FOR MULTI-CONNECTED DOMAINS

G. R. Baker* and M. J. Shelley*

Section I. Introduction

Various numerical techniques are available to compute solutions to elliptic partial differential equations. For specific equations, such as Laplace's equation, the biharmonic equation and Helmholtz's equation, boundary integral techniques have several advantages over standard finite-difference and finite-element techniques. Highly accurate solutions for even severely deformed geometries can be obtained easily by boundary integral techniques. For exterior problems, the far-field asymptotic boundary conditions are automatically satisfied. No special effort is required when the domain changes in time (or with some other independent parameter), since points on the boundary can be advanced in a straightforward fashion. In particular, generalized vortex methods, based on boundary integral techniques, have been used successfully to compute free surface motion of inviscid, incompressible fluid (Baker et al. 1980, 1982).

Several other researchers, such as Longuet-Higgins and Cokelet (1976) and Pullin (1982), have also used boundary integral techniques to study free surface motion. They used costly direct matrix inversion techniques to solve the integral equations, which take $O(N^3)$ operatons to perform where N is the number of points that represent the boundary. In contrast, Baker et al. (1982) realized that a suitable choice of source or dipole distributions along

*Department of Mathematics, University of Arizona, Tucson, Arizona 85710

Partially sponsored by the United States Army under Contract No. DAAG29-80-C-0041, the National Science Foundation, Grant No. MCS-8302549, and by NASA, Grant No. NGT 03002800.

the surface will lead to Fredholm integral equations of the second kind that may be solved iteratively in $O(N^2)$ operations. In simply-connected domains, the solution to Laplace's equation with Dirichlet boundary conditions may be found iteratively when a dipole distribution along the boundary is used. In multi-connected domains, an external source contribution must be added to the dipole distribution along the boundary as a representation for the velocity potential. This paper will describe how iterative techniques may be used to find both the source strength and the dipole distribution. Several test examples are solved numerically. In general, standard quadrature techniques provide accurate solutions to the boundary integral equations. However, when the multi-connected domain involves two non-intersecting surfaces that lie close together, interpolated quadrature techniques are used to solve the boundary integral equations accurately.

One application of these results is to the study of accelerating thin fluid shells. Baker (1983) has shown that the motion may be determined from the solution of Laplace's equation in a multi-connected domain with Dirichlet boundary conditions. Here the presence of the source term is crucial in determining correctly the dynamics of the motion. In some cases, it is known on other grounds that there is no flux across the surfaces and so no source term is necessary. This is relevant in studies of the classical Rayleigh-Taylor instability (Baker et al., 1980) and of the motion of water waves over variable bottom topography (Baker et al., 1982).

In Section II, we start by considering Laplace's equation exterior to a simply-connected domain. This simple case contains the essential features of the application of boundary integral equations for potential problems in multi-connected domains. In Section III, we consider Laplace's equation between two closed non-intersecting surfaces and finally, in Section IV, a numerical technique and results are presented.

Section II. The Exterior Problem

Consider the region $\overline{D}$ exterior to a simply-connected domain D with boundary ∂D. For convenience, the boundary will be assumed to have a continuous normal. Boundaries with corners introduce a slight modification in the mathematics (for details, see Jaswon and Symm, 1977). Suppose that the potential, ϕ, which satisfies Laplace's equation in $\overline{D}$, is specified along ∂D. In addition, the behavior of ϕ far from ∂D must be specified. In three-dimensions, a unique solution is determined by requiring that ϕ decays algebraically far from ∂D. However, in two-dimensions the situation is more complicated. A unique solution can be found if ϕ is logarithmic or tends to a constant at infinity but not both (Kellogg, 1929).

For simplicity of presentation, we shall assume that the potential is logarithmic at infinity if the geometry is two-dimensional. The other case is treated similarly. According to classical potential theory, ϕ may then be expressed in terms of a source distribution σ along ∂D;

$$\phi(p) = \int_{\partial D} \sigma(q) g(p,q) dq \quad , \qquad p \in \overline{D} \cup \partial D \tag{2.1}$$

where p and q are field points and $g(p,q)$ is the Green's function for Laplace's equation in free-space. In particular, when $p \in \partial D$, equation (2.1) constitutes a Fredholm equation of the first kind for the source strength σ in terms of the specified potential ϕ. If collocation and numerical quadrature are used to solve equation (2.1), a matrix equation results which is usually solved by direct inversion techniques. We are not aware of any matrix splitting that leads to an iteration scheme that converges globally, that is, converges for any choice of ∂D. Once σ is determined, ϕ can be evaluated in $\overline{D}$ via (2.1).

Alternatively, as suggested by the form of a solution for an interior Dirichlet problem, we may seek to express ϕ in terms of a dipole distribution μ along ∂D. However, such a representation is not sufficient. A dipole distribution decays to zero at infinity, and a source term must be added in order to satisfy the condition there. The location of the source inside ∂D is arbitrary but for numerical computations it is best not to place it near ∂D. For convenience, the source may be considered to be at the origin of the coordinate system. Thus

$$\phi(p) = \int_{\partial D} \mu(q) \frac{\partial g}{\partial n_q}(p,q)dq + A\phi_s(p) \quad , \quad p \in \overline{D} \cup \partial D \qquad (2.2)$$

where n is the normal pointing into $\overline{D}$ and the normal derivative is taken with respect to q (hence the q subscript on n). The unit source potential $\phi_s(p)$ depends on the nature of ∂D and the spatial dimension. In particular, for a closed ∂D in two dimensions,

$$\phi_s(p) = \frac{1}{2\pi} \log|p| . \qquad (2.3)$$

Clearly, equations for μ and A must be sought.

As p approaches ∂D along the normal, (2.2) takes on the limiting form

$$\oint_{\partial D} \mu(q) \frac{\partial g}{\partial n_q}(p,q)dq - \frac{\mu(p)}{2} = \phi(p) - A\phi_s(p) \equiv R(p), \; p \in \partial D \qquad (2.4)$$

Equation (2.4) has been written explicitly in the form of a Fredholm integral equation of the second kind for μ. The arbitrariness in A is only apparent in that the Fredholm alternative must be satisfied in order for (2.4) have a solution μ. As required by Fredholm theory, the eigenvalues λ of the equation,

$$2\lambda \oint_{\partial D} \mu(q) \frac{\partial g}{\partial n_q}(p,q)dq - \mu(p) = 0, \tag{2.5}$$

must be known. Kellogg (1929) proves that the eigenvalues are distinct and real and they all satisfy $|\lambda| \geq 1$. In addition, $\lambda = 1$ is an eigenvalue of geometric multiplicity one with eigenvector $\mu = C$, a constant (Jaswon and Symm, 1977). This corresponds to a potential distribution $\phi = C$ in D and $\phi = 0$ in $\bar{D}$.

Since (2.4) has a non-trivial solution when $R = 0$ there is no solution to (2.4) for $R \neq 0$ unless R satisfies the Fredholm alternative. Multiply (2.4) by a source distribution $\sigma(p)$ along ∂D and integrate around ∂D with respect to p. The result may be written as

$$\int_{\partial D} \mu(q)\left[\oint_{\partial D} \sigma(p)\frac{\partial g}{\partial n_q}(p,q)dp - \frac{\sigma(q)}{2}\right]dq = \int_{\partial D} R(p)\sigma(p)dp \tag{2.6}$$

In particular, if σ is a nontrivial solution of the adjoint problem,

$$\oint_{\partial D} \sigma(q) \frac{\partial g}{\partial n_p}(p,q)dq - \frac{\sigma(p)}{2} = 0, \tag{2.7}$$

then

$$\int_{\partial D} R(p)\sigma(p)dp = 0, \tag{2.8}$$

where the following relationship has been used;

$$g(p,q) = g(q,p). \tag{2.9}$$

Clearly, (2.8) is a necessary condition for μ to exist. The fact that it is also a sufficient condition follows from the usual method of proof that establishes the Fredholm alternative (see Mikhlin, 1957). The Fredholm alternative also guarantees that there exists only one nontrivial σ which satisfies (2.7) aside from a multiplicative constant.

Provided R satisfies (2.8), there is a solution μ for (2.4) which is arbitrary to the addition of any constant $\bar{\mu}$. Fortunately, a constant $\bar{\mu}$ corresponds to a constant potential in D and zero potential in $\bar{D}$. In most physical applications, such as incompressible, inviscid irrotational fluid flow, it is $\nabla\phi$ that is important and any constant $\bar{\mu}$ may be ignored.

Finally, note that condition (2.8) becomes, upon substitution for R from (2.4),

$$A \int_{\partial D} \phi_s(p)\sigma(p)dp = \int_{\partial D} \phi(p)\sigma(p)dp \tag{2.10}$$

which is an equation for A. Thus, a nontrivial σ is determined from (2.7) and (2.10) is then used to determine A. Next (2.4) is solved for μ with any additional constraint that eliminates the arbitrariness in μ. For example, one may specify the value of μ at a point on ∂D;

$$\mu(p_0) = 0. \tag{2.11}$$

At first sight, equations (2.4), (2.7) and (2.10) appear to introduce greater computational complexity than (2.1). However both (2.4) and (2.7) may be solved iteratively. Let $\mu^{(n)}(p)$ be the nth iterative and obtain the next iterative from

$$\mu^{(n+1)}(p) = T\mu^{(n)}(p) - T\mu^{(n)}(p_0) \tag{2.12a}$$

where

$$T\mu(p) = 2\int_{\partial D} \mu(q)\frac{\partial g}{\partial n_q}(p,q)dq - 2R(p). \tag{2.12b}$$

As $n \to \infty$, $\mu^{(n)} \to \mu$, the solution to (2.4) subject to (2.11). Similarly, an iteration procedure for σ may be used where for convenience the additional constraint,

$$\max_{p \in \partial D} |\sigma(p)| = 1 \tag{2.13}$$

is imposed to remove the arbitrary multiplicative constant in σ. The convergence of the iteration scheme follows from the global convergence of the Neumann series for both integral equations. A proof follows from the proof given in Baker et al (1982) for the case of open periodic surfaces. In particular, for time dependent domains the iteration is very efficient since a good first guess is always available from information at the previous time value, and, if information from previous time levels is retained, extrapolation further improves the first guess. If the solution ϕ to the two-dimensional Laplace's equation is being sought in D subject to ϕ tending to a constant at infinity, $\phi_s(p) = 1$ must be used in place of (2.3) and the source distribution in (2.1) must be modified (Jaswon and Symm, 1977).

As shown in the simple case above, the Fredholm alternative lies at the heart of the application of dipole distributions to the solution of Laplace's equation in multi-connected domains. In the next section, a more general multi-connected domain will be considered and then numerical results will be presented in the following section.

Section III The Annular Problem

Consider the multi-connected domain as shown schematically in Figure 1. Domain D_2 lies between two closed, non-intersecting surfaces ∂D_1 and ∂D_2 with ∂D_1 enclosing ∂D_2. The exterior domain $\bar{D}$ is composed of two parts, D_3 internal to ∂D_2 and D_1 external to ∂D_1. Once again, ∂D_1 and ∂D_2 are assumed to have continuous normals.

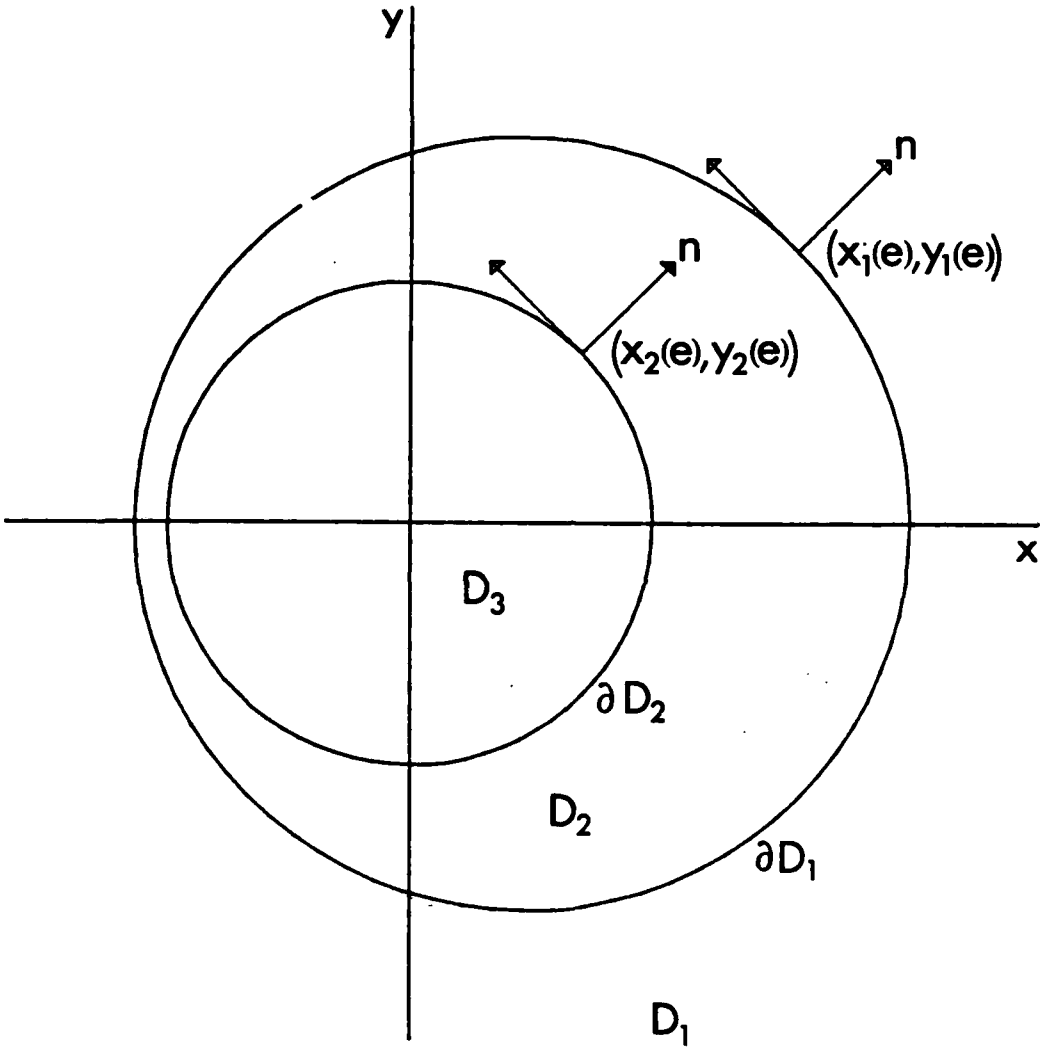

Figure 1. Schematic showing the assumed notation for an annulus.

To be specific and for convenience, suppose that a solution to the two-dimensional Laplace's equation is sought in D_2 with Dirichlet boundary conditions imposed at ∂D_1 and ∂D_2. Following the procedure adopted in Section II, the solution is expressed in terms of a source term and dipole distributions along ∂D_1 and ∂D_2;

$$\phi(p) = \frac{A}{2\pi}\log|p| + \sum_{j=1}^{2} \int_{\partial D_j} \mu_j(q) \frac{\partial g}{\partial n_q}(p,q)dq, \quad p \in D_2 . \tag{3.1}$$

Let ∂D_1 and ∂D_2 be parameterised in a counter-clockwise direction by $(x_1(e),y_1(e))$ and $(x_2(e),y_2(e))$ respectively. In free-space, the two-dimensional Green's function is $\frac{1}{4\pi}\log\{(x-x_k)^2 + (y-y_k)^2\}$ where (x_k,y_k) locates the source point on ∂D_k . The normal derivative of the Green's function evaluated at the kth surface has the form

$$K_{jk}(e,e') = \frac{1}{2\pi} \frac{x_{ke}(e')\{y_j(e)-y_k(e')\}-y_{ke}(e')\{x_j(e)-x_k(e')\}}{\{x_j(e)-x_k(e')\}^2+\{y_j(e)-y_k(e')\}^2}, \tag{3.2}$$

where the subscript e denotes differentiation and the field point lies on the jth surface.

The evaluation of (3.1) at ∂D_1 and ∂D_2 gives two coupled Fredholm integral equations for μ_1 and μ_2:

$$\lambda \oint_{\partial D_1} \mu_1(e')K_{11}(e,e')de' + \lambda \int_{\partial D_2} \mu_2(e')K_{12}(e,e')de' + \frac{\mu_1(e)}{2}$$

$$= \phi_1(e) - \frac{A}{4\pi}\log\{x_1^2(e) + y_1^2(e)\} \tag{3.3a}$$

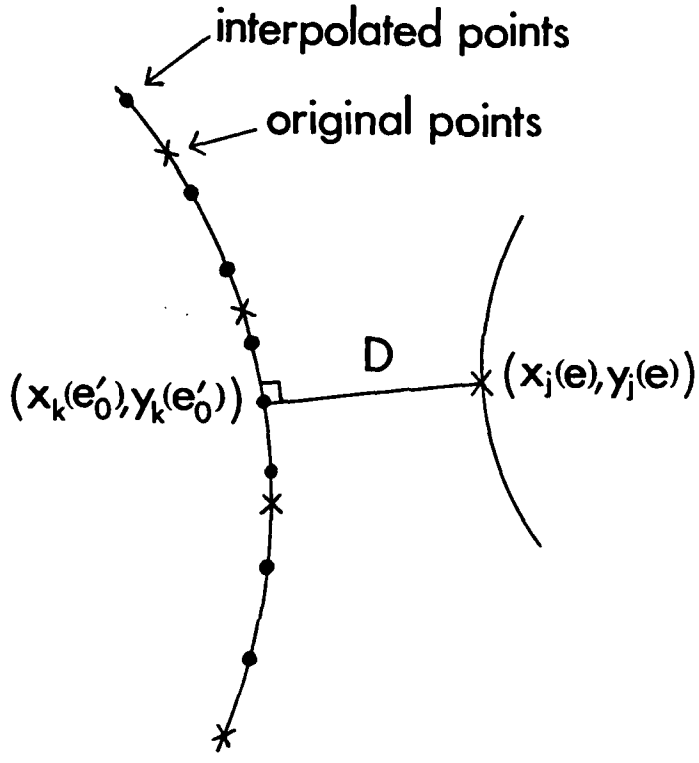

Figure 3. Schematic showing notation for regions where the annulus is thin.

defined by the requirement that $(x_k(e'_0), y_k(e'_0))$ is the closest point on surface k to $(x_j(e), y_j(e))$. Figure 3 gives a schematic of the situation. The value e'_0 may be found by using interpolation and Newton iteration to locate the minimum distance. To resolve the peak or trough, N points are interpolated along the surface in the following way. Given that points $(x_k(e'), y_k(e'))$ are originally assigned by evenly spaced intervals in e', N new points are obtained by taking evenly spaced intervals in $\hat{e}$, where

$$e' = \hat{e} + \alpha \sin(\hat{e} - e'_0) \tag{4.13}$$

and $\hat{e} = e'_0$ gives one of the new points. The trapezoidal rule is used with the new points; quantities such as τ and μ are also interpolated to be able to evaluate the integrand. Note that the same number of points N are used. Clearly, the choice of α will dictate the accuracy. Note that interpolation must be done whenever a point on the jth surface is too close to the kth surface.

The error $\bar{E}$ for the circular case may be analysed in more general terms to estimate its behavior for other geometries. For large N, the error $\bar{E}$ is most strongly affected by the term ρ^{-N}, provided $\rho \neq 1$. When $j = 1$ and $k = 2$, the error is associated with the approximation to the integral involving $K_{12}(e,e')$. Set $R_2 = R$ and $R_1 = R+D$. Then,

$$\begin{aligned} \rho^{-N} &= (1 + D/R)^{-N} \\ &= \exp(-N \log(1 + D/R)) \\ &\approx \exp(-2\pi D/\Delta S(1 + D/2R)) \end{aligned} \tag{4.14}$$

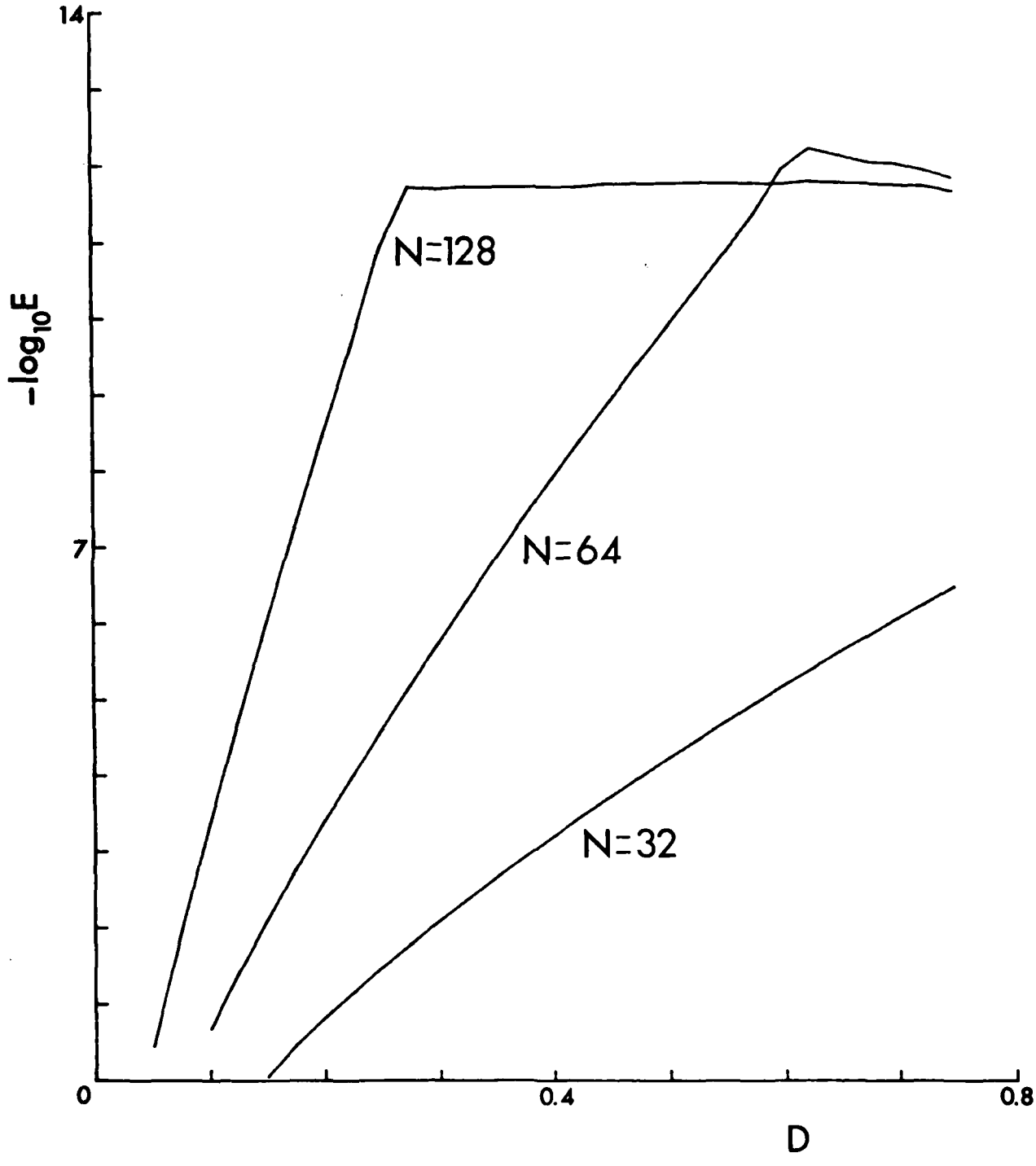

Figure 2. The maximum of the absolute error E in dipole sheet strength for the circular annulus as D is varied, where D is the thickness of the annulus.

is quite small. Incidentally, the mode $m = 16$ cannot be resolved by the numerical quadrature since alternate points were used so $m = 15$ is the highest mode realistically treated by the quadrature. The maximum number of iterations required occurs when $m = 1$ and the number decreases for larger values of m, consistent with other iterative, numerical techniques used to solve elliptic problems. Clearly, multi-grid techniques may be used to reduce strongly the required number of iterations, but we have not pursued that aspect here. The numerically calculated value for the source strength A was always within roundoff error of its exact value.

Unfortunately there are times when straightforward use of the numerical procedure described above will result in errors of $O(1)$. From (4.12), it is easy to see that E is $O(1)$ when R_1 and R_2 are very close together. Figure 2 displays the behavior of E as the width of the circular annulus is decreased in the test case (4.4-6). Here $R_1 = 1+D$, $R_2 = 1$, $m = 1$, $N_1 = N_2 = N$, and an absolute tolerance of 10^{-12} was used for the convergence of the iterations, (3.7) and (3.8). Clearly for a fixed number of discretisation points N, the strong variation in the integrand K_{jk}, $j \neq k$, is not well resolved when a point on one surface is close to the other surface along which the integral is performed. The error begins to downgrade noticeably when the thickness D of the annulus is sufficiently small. This error has been previously observed by Maskew (1977) in a related calculation involving vortex sheet motion. Clearly, as Maskew points out, more points are required to resolve the strong variation of the integrand, and as N is increased for fixed D accuracy improves dramatically.

It is expensive and unnecessary to increase N substantially for accuracy when D is small . Consider a point $(x_j(e),y_j(e))$ near surface k. The integrand $K_{jk}(e,e')$ has a sharp peak or trough centered around e'_0 ,

N	m	Error	I_μ
16	1	0.305×10^{-3}	26
32	1	0.466×10^{-8}	26
64	1	0.117×10^{-11}	26
32	2	0.528×10^{-8}	14
32	4	0.160×10^{-7}	8
32	8	0.239×10^{-6}	5
32	12	0.382×10^{-5}	4
32	15	0.305×10^{-4}	3

Table I: Results for the circular annulus as described in the test. $I_\tau = 2$ in all cases.

$$\mu_2 = (2 + \bar{E})\ (\cos\ (jmh) - 1) \qquad (4.11b)$$

where

$$\bar{E} = \frac{2(\rho^m + \rho^{-m})}{\rho^N - \rho^{N-m} - \rho^m - 1}\ , \qquad (4.12)$$

and $\rho = R_1/R_2$.

A numerical code has been written that solves the Dirichlet problem for a general annulus (not necessarily circular). In particular, the code was applied to the test case described above. Results are shown in Table I when $R_1 = 2$, $R_2 = 1$, and $N_1 = N_2 = N$ points are used. The reported error E is the maximum absolute difference between the computed dipole strengths and the exact values given in (4.7); theoretically this error should be $2|\bar{E}|$ and the agreement is perfect as long as the error is above the absolute tolerance of 10^{-12} used to determine convergence of the iteration scheme. Also tabulated are the number of iterations I_τ and I_μ required to solve the integral equations for τ_j and μ_j respectively to within the absolute tolerance. We emphasize that the error arises solely from the numerical approximation to the integral that determines the contribution to the field point on one surface from the dipole distribution along the other surface. For $m = 1$, there is a dramatic improvement in accuracy as N increases reflecting the infinite order of the trapezoidal rule on periodic integrands. Already, for $N = 64$, the error is below the tolerance required. Of course, this result is not too surprising since a circular annulus has been chosen, but later results will be represented for elliptic annuli that still show the high accuracy of the method. As the mode number m of the potential is increased with fixed N, the resolution of the integrand deteriorates, but even for $m = 15$, the error

The eigenvectors for the discrete equations that represent (3.5) are proportional to cos(mjh) and sin(mjh). In particular, for $m = 0$, the eigenvalue, which corresponds to $\lambda = 1$ in the continuous case, is

$$\lambda = \frac{R_1^N - R_2^N}{R_1^N + R_2^N} \tag{4.9}$$

and the numerically calculated eigenvector is $\tau_1 = 1$, $\tau_2 = -1$, which is exact. When these values for τ_1, τ_2 are substituted into (3.4) and the trapezoidal rule is used to compute the integrals in (3.4), the numerically determined value for A is also exact, that is $A = 1$.

Next, the error in solving (3.3) can be computed. The following sums,

$$\mathrm{Re}\left\{ \frac{2}{N} \sum_{\substack{k=0 \\ k+j \text{ odd}}}^{N-1} \frac{\cos(kmh)\, e^{ikh}}{e^{ijh} - e^{ikh}} \right\} = \begin{cases} 0 & \text{for } m \neq 0 \\ -\frac{1}{2} & \text{for } m = 0 \end{cases} \tag{4.10a}$$

$$\mathrm{Re}\left\{ \frac{R_2}{N} \sum_{k=0}^{N-1} \frac{\cos(kmh)\, e^{ikh}}{R_1 e^{ijh} - R_2 e^{ikh}} \right\} = \frac{1}{2} \frac{R_1^m R_2^{N-m} + R_1^{N-m} R_2^m}{R_1^N - R_2^N} \cos(jmh), \quad m \neq 0$$

$$\frac{R_2^N}{R_1^N - R_2^N}, \quad m = 0 \tag{4.10b}$$

give the trapezoidal approximation for the various integrals in (3.3). Once again, (4.10a) implies that the principal-value integrals are computed exactly and errors come only from the approximation to the other integrals. It is a straightforward calculation to find the numerically determined dipole sheet strengths,

$$\mu_1 = (2 + \bar{E})\,(\cos(jmh) - 1) \tag{4.11a}$$

$$\phi_1(e) = \left(1 - \left(\frac{R_2}{R_1}\right)^m\right) \cos(me) + \log(R_1) \qquad (4.6a)$$

$$\phi_2(e) = \left(\left(\frac{R_2}{R_1}\right)^m - 1\right) \cos(me) + \log(R_2) \qquad (4.6b)$$

on the boundaries ∂D_1 and ∂D_2 respectively. The exact values for the dipole sheet strengths such that $\mu_1(o) = \mu_2(o) = 0$ are

$$\mu_1(e) = \mu_2(e) = 2\,[\cos(me) - 1]. \qquad (4.7)$$

For this simple test case, the error involved in using trapezoidal quadrature can be calculated exactly. The following sums

$$\mathrm{Re}\left\{\frac{2}{N} e^{ijh} \sum_{\substack{k=0 \\ k+j \text{ odd}}}^{N-1} \frac{\cos(kmh)}{e^{ijh} - e^{ikh}}\right\} = \begin{cases} 0, & \text{for } m \neq 0 \\ 1/2 & \text{for } m = 0 \end{cases} \qquad (4.8a)$$

$$\mathrm{Re}\left\{R_1 e^{ijh} \sum_{k=0}^{N-1} \frac{\cos(kmh)}{R_1 e^{ijh} - R_2 e^{ikh}}\right\} = \frac{1}{2} \frac{R_1^m R_2^{N-m} + R_1^{N-m} R_2^m}{R_1^N - R_2^N} \cos(jmh), \quad m \neq 0$$

$$\frac{R_1^N}{R_1^N - R_2^N}, \quad m = 0 \qquad (4.8b)$$

where $h = 2\pi/N$ and $0 \leq m < \frac{N}{2}$, give the trapezoidal approximation to the various integrals in (3.5) where N evenly spaced points have been used to represent each surface. The sum (4.8a) which approximates the principal-value integrals, gives the exact analytic result, reflecting the spectral accuracy of the trapezoidal rule. Thus the only errors arise from the sums (4.8b) that approximate the integrals along the surface opposite to the one containing the field point, $(x_j(e), y_j(e))$, in $K_{jk}(e,e')$ in (3.2).

The trapezoidal rule is applied as follows. N_j points are selected at evenly spaced intervals in e to represent surface ∂D_j. At each such point, e_i say, in (3.7) and (3.8) as modified by (4.2) and (4.3), $T_j(e_i)$ must be calculated. One integral involves contributions from the other surface and the trapezoidal rule may be applied directly. For the integral along ∂D_j however, application of the trapezoidal rule would require evaluation of the integrand at $e' = e_j$ which is an indeterminant form. The limiting value is easily calculated but involves derivatives of the dipole sheet strength and the surface. Instead, it is more convenient to apply the trapezoidal rule on alternate points so that $e' = e_k$ for all k such that $k + j$ is odd. Clearly, a quadrature point never falls on e and the integrand is always easily computed. A disadvantage to this procedure is a slight loss of resolution of the integrand. Tests will show that this is not important in most cases.

As a simple test, consider the annulus lying between the circles defined by

$$x_1 = R_1 \cos(e), \qquad y_1 = R_1 \sin(e) \tag{4.4a}$$

and

$$x_2 = R_2 \cos(e), \qquad y_2 = R_2 \sin(e) \tag{4.4b}$$

where R_1 and R_2 are constants. A solution to Laplace's equation in polar coordinates (r, θ) in the annulus is

$$\phi = \left(\left(\frac{r}{R_1}\right)^m - \left(\frac{R_2}{r}\right)^m\right) \cos(m\theta) + \log(r) \tag{4.5}$$

which takes on the values

$$\int_{\partial D_j} K_{jj}(e,e')\, de' = \frac{1}{2} . \tag{4.1}$$

Thus the integrals in (3.7) may be replaced by

$$-2\int_{\partial D_1} \{\mu_1^{(n)}(e') - \mu_1^{(n)}(e)\}\, K_{11}(e,e')\, de' - \mu_1^{(n)}(e)$$

$$-2\int_{\partial D_2} \mu_2^{(n)}(e')\, K_{12}(e,e')\, de' \tag{4.2a}$$

and

$$2\int_{\partial D_2} \{u_2^{(n)}(e') - \mu_2^{(n)}(e)\}\, K_{22}(e,e')\, de' + \mu_2^{(n)}(e)$$

$$+2\int_{\partial D_1} \mu_1^{(n)}(e')\, K_{21}(e,e')\, de' \tag{4.2b}$$

These integrals have smooth, periodic integrands and may thus be evaluated accurately by the trapezoidal rule. Indeed, the accuracy is infinite order or spectral (Isaacson and Keller, 1966). Similarly, the integrals in (3.8) may be replaced by

$$\int_{\partial D_1} \{\tau_1^{(n)}(e')\, G_{11}(e,e') - \tau_1^{(n)}(e)\, K_{11}(e,e')\}\, de' + \frac{1}{2}\tau_1^{(n)}(e)$$

$$+\int_{\partial D_2} \tau_2^{(n)}(e')\, G_{12}(e,e')\, de', \tag{4.3a}$$

$$\int_{\partial D_2} \{\tau_2^{(n)}(e')\, G_{22}(e,e') - \tau_2^{(n)}(e)\, K_{22}(e,e')\}\, de' - \frac{1}{2}\tau_2^{(n)}(e)$$

$$-\int_{\partial D_1} \tau_1^{(n)}(e')\, G_{21}(e,e')\, de' . \tag{4.3b}$$

$$T_2(\tau_1,\tau_2)(e) = -\int_{\partial D_1} \tau_1(e')\, G_{21}(e,e')\, de' - \int_{\partial D_2} \tau_2(e')\, G_{22}(e,e')\, de' - \tau_2(e) \qquad (3.8d)$$

and $T_m = \max_{j=1,2} T_j(\tau_1^{(n)},\tau_2^{(n)})(e)$. The disadvantage to shifting the eigenvalues is that the convergence rate is halved.

The above interation method is effectively a Neumann iteration method applied to the discrete version of the boundary integral equations. A referee has pointed out that a generalized conjugate residual algorithm might significantly improve the convergence (see Eisenstat et al. 1983). The basic conjugate gradient method was tried on the exterior problem with little gain in convergence, but we have not as yet tried the improved algorithm.

Clearly, the numerical implementation of the above procedure demands reliable and accurate evaluation of the integrals. In the next section, a numerical quadrature and results for some test cases are presented.

Section IV. Numerical Results

The design of a numerical quadrature for the integrals in (3.7) and (3.8) depends on several factors. Firstly, the kernels K_{jj} and G_{jj} are singular. Secondly, the smoothness of the surfaces ∂D_1 and ∂D_2 and of the boundary values ϕ_1 and ϕ_2 may affect the accuracy. Fortunately, for applications to studies of free surface flows, the surfaces and boundary values are generally C^∞ functions. Furthermore, for closed surfaces in two-dimensions, the singularities in K_{jj} and G_{jj} may be removed by using the identity,

$$T_2(\mu_1,\mu_2)(e) = 2 \int_{\partial D_1} \mu_1(e')K_{21}(e,e')de' + 2 \int_{\partial D_2} \mu_2(e')K_{22}(e,e')de' - 2\phi_2(e) + \frac{A}{2\pi} \log \{x_2^2(e) + y_2^2(e)\} \tag{3.7d}$$

will converge to values of μ_1 and μ_2 that are shifted by some constant value from the correct values. However the net effect of these shifts is to produce a corresponding constant shift in the potential distribution. Normally, such shifts in potential are not physically interesting. However, if necessary, it is a relatively simple matter to add the appropriate constant to the potential.

The iteration procedure for finding the eigenfunctions τ_1 and τ_2 that correspond to $\lambda = 1$ must be modified differently since the eigenfunctions τ_1 and τ_2 that correspond to $\lambda = -1$ are not known in general. Instead the eigenvalue $\lambda = -1$ is shifted to the origin by using the following iteration scheme;

$$\tau_1^{(n+1)}(e) = T_1(\tau_1^{(n)},\tau_2^{(n)})(e)/T_m \tag{3.8a}$$

$$\tau_2^{(n+1)}(e) = T_2(\tau_1^{(n)},\tau_2^{(n)})(e)/T_m \tag{3.8b}$$

where

$$T_1(\tau_1,\tau_2)(e) = \int_{\partial D_1} \tau_1(e')\, G_{11}(e,e')\, de' + \int_{\partial D_2} \tau_2(e')\, G_{12}(e,e')\, de' + \tau_1(e) \tag{3.8c}$$

$$G_{jk}(e,e') = - K_{kj}(e' e) \tag{3.6}$$

and τ is related to a source distribution σ by $\tau = \sigma s_e$ where s is the arclength.

The solution ϕ may now be calculated as follows. The solution to (3.5) yields τ_1 and τ_2 which are substituted into (3.4) so that A may be calculated. Thus (3.3) may be solved for μ_1 and μ_2 and ϕ may be evaluated from (3.1).

There remains the question of how to compute the solutions to (3.3) and (3.5). The observation has already been made that $\lambda = 1$ is an eigenvalue to the homogeneous equations associated with (3.3). There is also an eigenvalue $\lambda = -1$ with $\mu_1 = C$, $\mu_2 = -C$, which corresponds to a potential distribution $\phi = 0$ in D_1 and D_3 and $\phi = C$ in D_2. Unfortunately the eigenvalue $\lambda = -1$ affects the iteration scheme that arises naturally by the generalization of (2.12). Since all other eigenvalues satisfy $|\lambda| > 1$ (see Kellogg, 1929), the eigenvalues $\lambda = \pm 1$ are the only ones that prevent convergence of the iteration scheme. Thus the modified iteration scheme,

$$\mu_1^{(n+1)}(e) = T_1(\mu_1^{(n)},\mu_2^{(n)})(e) - T_1(\mu_1^{(n)},\mu_2^{(n)})(0) \tag{3.7a}$$

$$\mu_2^{(n+1)}(e) = T_2(\mu_1^{(n)},\mu_2^{(n)})(e) - T_2(\mu_1^{(n)},\mu_2^{(n)})(0) \tag{3.7b}$$

where

$$\begin{aligned} T_1(\mu_1,\mu_2)(e) = &-2\int_{\partial D_1} \mu_1(e')K_{11}(e,e')de' - 2\int_{\partial D_2} \mu_2(e')K_{12}(e,e')de' \\ &+ 2\phi_1(e) - \frac{A}{2\pi} \log \{x_1^2(e) + y_1^2(e)\}, \end{aligned} \tag{3.7c}$$

$$\lambda \int_{\partial D_1} \mu_1(e')K_{21}(e,e')de' + \lambda \oint_{\partial D_2} \mu_2(e')K_{22}(e,e')de' - \frac{\mu_2(e)}{2}$$

$$= \phi_2(e) - \frac{A}{4\pi} \log \{x_2^2(e) + y_2^2(e)\} \qquad (3.3b)$$

where $\phi_1(e)$ and $\phi_2(e)$ are the values imposed on ϕ at ∂D_1 and ∂D_2 respectively. The origin of the coordinate system has been chosen to coincide with the location of the source point inside D_3 of strength A. Although $\lambda = 1$, it has been introduced to facilitate the discussion on the existence of solutions for μ_1 and μ_2 and the global convergence of the Neumann series for the integral equations.

When $\lambda = 1$, $\mu_1 = 0$ and $\mu_2 = C$, a constant, are solutions to the homogeneous equations ($\phi_1 = \phi_2 = A = 0$) corresponding to a potential distribution $\phi = 0$ in D_1 and D_2, $\phi = C$ in D_3. This eigenvalue is closely associated to that in (2.5). According to Fredholm's theorem of the alternative, (3.3) has a solution provided

$$\frac{A}{4\pi} \left[\int_{\partial D_1} \tau_1(e) \log \{x_1^2(e) + y_1^2(e)\} \, de + \int_{\partial D_2} \tau_2(e) \log \{x_2^2(e) + y_2^2(e)\} de \right]$$

$$= \int_{\partial D_1} \phi_1(e)\tau_1(e) \, de + \int_{\partial D_2} \phi_2(e)\tau_2(e) \, de \, , \qquad (3.4)$$

where τ_1 and τ_2 satisfy the homogeneous, adjoint equations

$$\oint_{\partial D_1} \tau_1(e') \, G_{11}(e,e') \, de' + \int_{\partial D_2} \tau_2(e') \, G_{12}(e,e') \, de' - \frac{\tau_1(e)}{2} = 0 \qquad (3.5a)$$

$$\int_{\partial D_1} \tau_1(e') \, G_{21}(e,e') \, de' + \oint_{\partial D_2} \tau_2(e') \, G_{22}(e,e') \, de' + \frac{\tau_2(e)}{2} = 0 \qquad (3.5b)$$

Here

where the quantity ΔS is the arc length between points and so $N\Delta S = 2\pi R$. This result in (4.14) is obtained by rewriting $D/R = 2\pi D/N\Delta S$ and considering $D/\Delta S$ fixed for large N. The approximation $z/(1 + z/2)$ to $\log(1 + z)$ is used rather than $z(1 - z/2)$. We found that this modification gave better agreement with the numerical results reported later.

For the other case, $j = 2$ and $k = 1$; set $R_1 = R$, $R_2 = R-D$ and $N\Delta S = 2\pi R_2$. Now,

$$\rho^{-N} = (1 - D/R)^{+N} \approx \exp(-2\pi D/(\Delta S(1 - D/2R))). \qquad (4.15)$$

The factors $1 \pm D/2R$ in (4.14) and (4.15) are curvature $|\kappa| = 1/R$ corrections to the expression $\exp(-2\pi D/\Delta S)$ which describes the influence of the error as a field point approaches a flat surface containing a dipole distribution (the error for this case is also easily calculated). In general, the correction can be written as $1 + D|\kappa|/2$, $1 - D|\kappa|/2$ depending upon whether the region of the surface nearest the point appears convex (see Figure 2) or concave respectively. In Figure 4, we replot the error as a function of $D/(\Delta S(1 - D|\kappa|/2))$ where Δs and κ is determined on the outer surface. Clearly, the asymptotic form (4.15), while not strictly valid for all values of D, does capture the essential behavior of E.

To decrease the error, the local $\bar{\Delta S}$ between the new, interpolated points should be given by

$$\frac{D}{\bar{\Delta S}} \Big/ \left(1 \pm \frac{D|\kappa|}{2}\right) = C, \qquad (4.16)$$

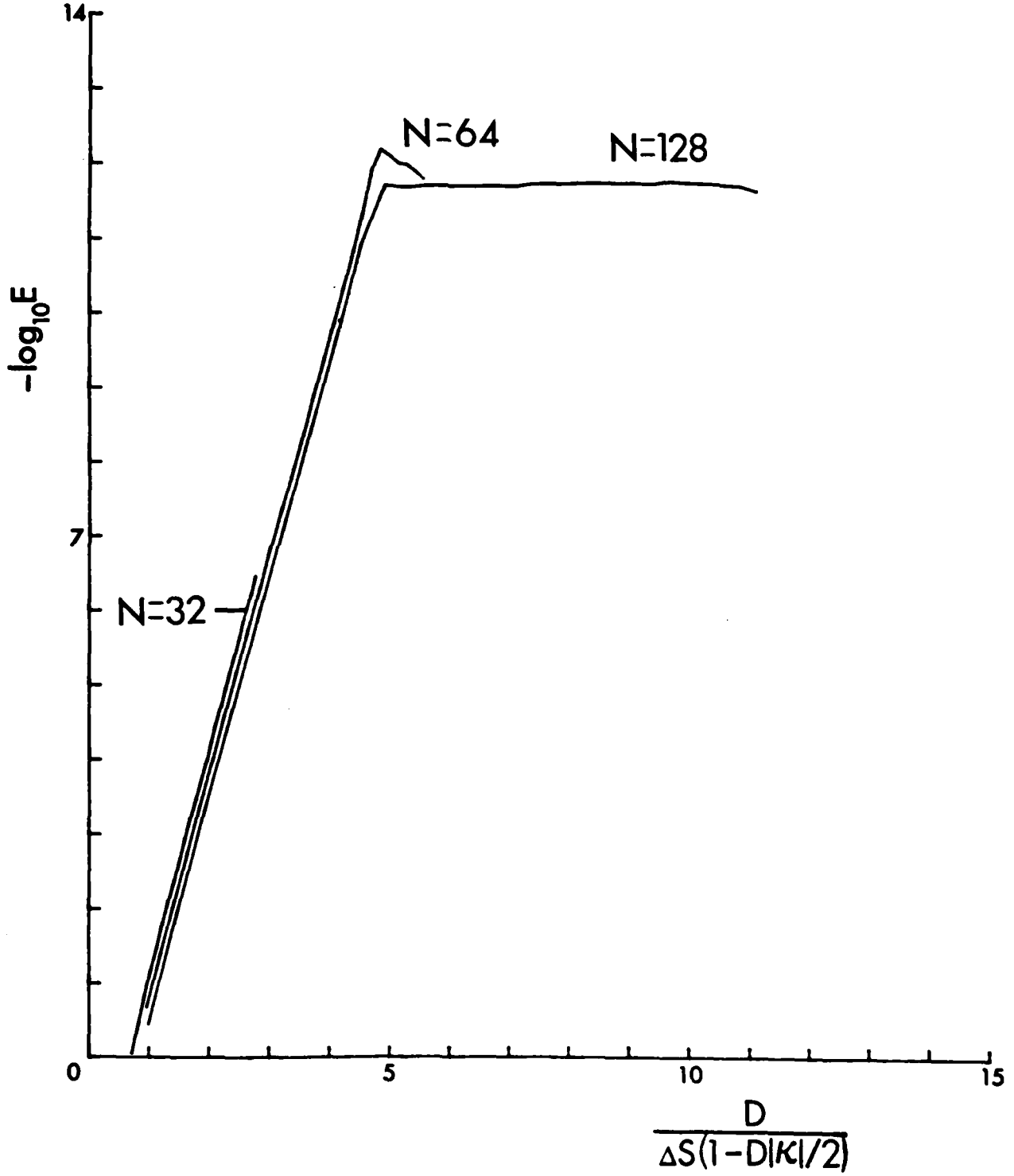

Figure 4. The same as Figure 2 except D is scaled by $\Delta S(1-d|\kappa|/2)$ where the local arclength between points, ΔS, and κ are measured on the outer boundary.

where C is a constant, chosen by experimentation to give the required accuracy. From (4.13), it is easy to determine the new $\overline{\Delta S}$ in terms of α,

$$\overline{\Delta S} = \Delta S(1 + \alpha). \tag{4.17}$$

Consequently, α has the form

$$\alpha = \frac{D}{C\Delta S}/(1 \pm \frac{D|\kappa|}{2}) - 1. \tag{4.18}$$

In Figure 5, the error is shown as D is varied for the same test case as shown in Figure 2, but now interpolated points are used whenever $\alpha > 0$ in (4.18). Interpolation was done using a discrete Fourier representation for which $C = 9.0$ was found to be a good choice. For small D, the errors are essentially the same as for larger D except for extremely small values of D, when the interpolated points are all clustered near e_0 and there are effectively no points resolving the rest of the surface. This effect clearly depends on N.

In some cases, such as a "noisy" representation of the surface, Fourier interpolation is inappropriate. In such cases, cubic spline interpolation may be used and we show the results in Figure 6. Because of the errors involved in using cubic splines, the error can be no better than $O(\Delta e^4)$. Now there is a transition from spectral accuracy to $O(\Delta e^4)$ as D becomes small and interpolated points are used. For this case, $C = 6.0$ since the accuracy is limited and there is no point in using interpolated points for a large value of C.

Finally, we demonstrate that these results are not special to a circular annulus but hold true for generally shaped annuli. Take the boundaries of the

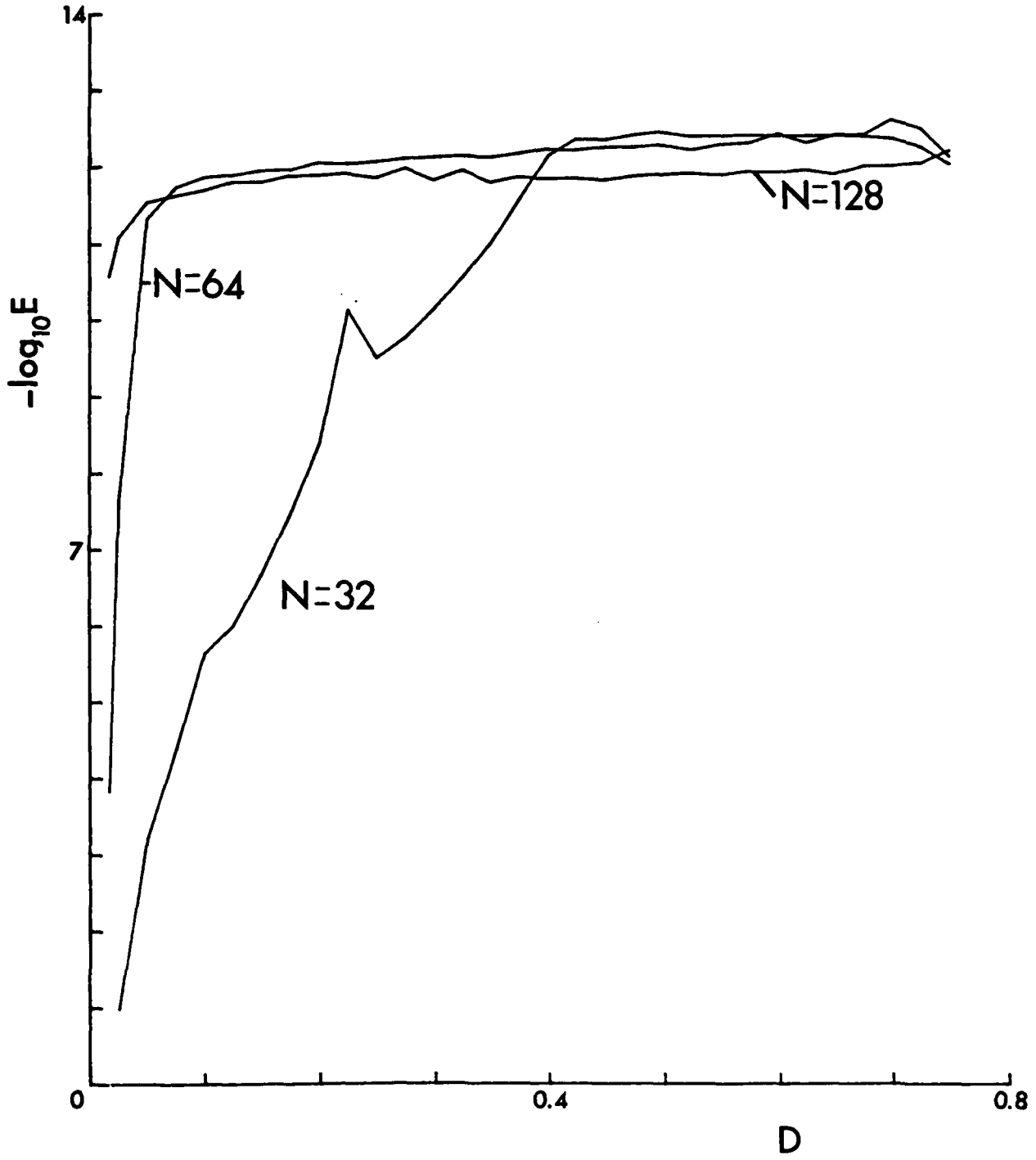

Figure 5. The maximum of the absolute error E in dipole sheet strength for the circular annulus as a function of D when Fourier interpolation is used to redistribute quadrature points.

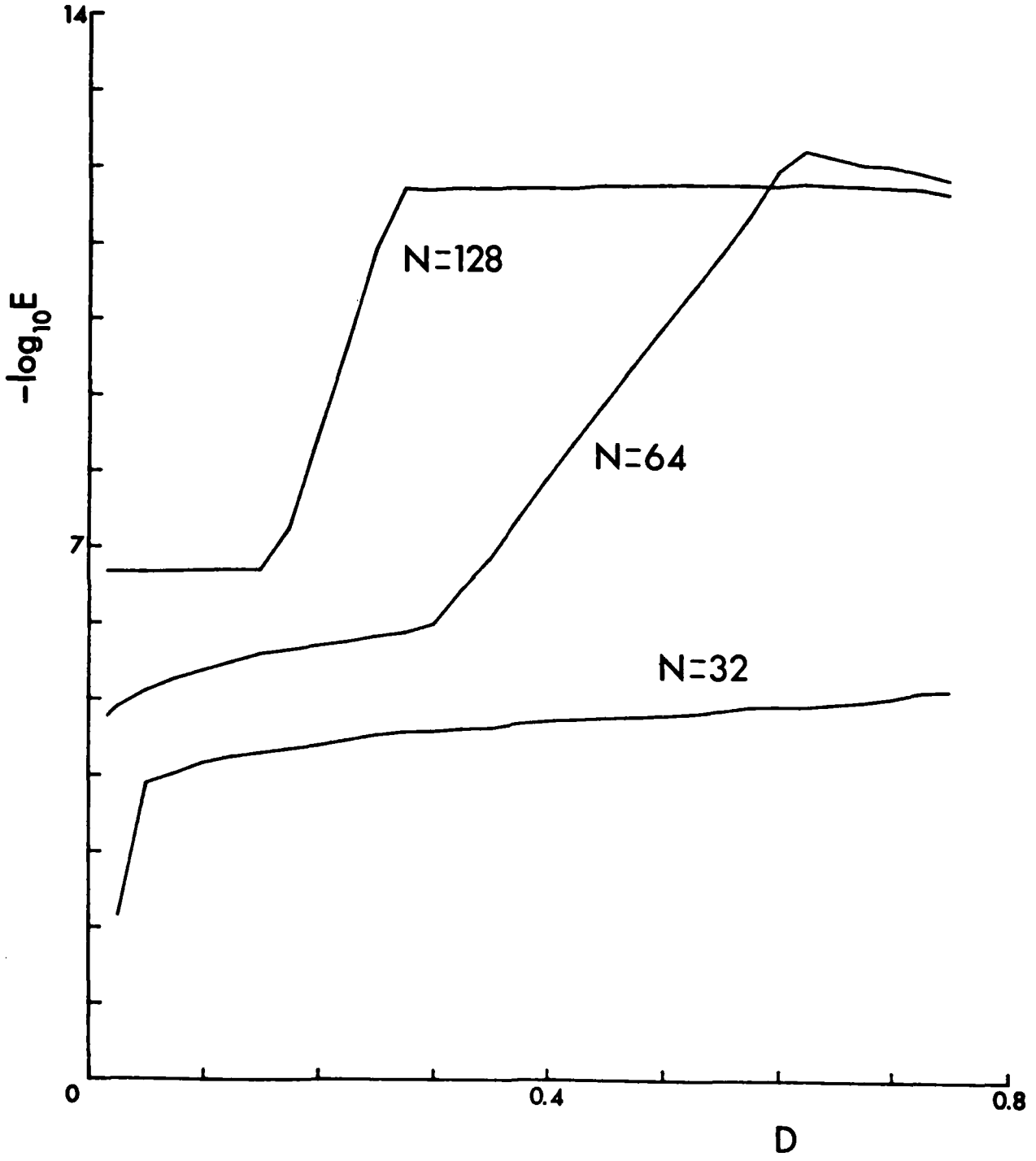

Figure 6. The same as Figure 5, except cubic spline interpolation is used.

annuli to be the following ellipses,

$$x_1 = r \cos(e) \tag{4.19a}$$

$$y_1 = (r^2 - 3/4)^{1/2} \sin(e), \tag{4.19b}$$

and

$$x_2 = \cos(e) \tag{4.20a}$$

$$y_2 = \frac{1}{2} \sin(e) \ . \tag{4.20b}$$

Our tests keep the inner boundary fixed and vary the outer boundary by changing r. The conformal map,

$$x + iy = \frac{\sqrt{3}}{2} \cosh(\zeta + i\eta), \tag{4.21}$$

transforms the elliptic annulus into a circular one and so an exact solution for the Dirichlet problem can be found. In particular, we chose the boundary conditions,

$$\phi_1 = (\alpha \cosh(2\zeta_1) + \beta \sinh(2\zeta_1)) \cos(2e) \tag{4.22a}$$

$$\phi_2 = (\frac{5}{3} \alpha + \frac{4}{3} \beta) \cos(2e) \ , \tag{4.22b}$$

where

$$\alpha = -\beta - \bar{\mu}_1/(\cosh(2\zeta_1) + \sinh(2\zeta_1)) \tag{4.23a}$$

$$\beta = -\frac{4}{3}\bar{\mu}_2 \tag{4.23b}$$

$$\cosh(\zeta_1) = \frac{2r}{\sqrt{3}} \tag{4.23c}$$

$$\sinh(\zeta_1) = (4r^2/3 - 1)^{1/2} \tag{4.23d}$$

and the corresponding dipole strengths are

$$\mu_1 = \bar{\mu}_1 \cos(2e) \tag{4.24a}$$

$$\mu_2 = \bar{\mu}_2 \cos(2e) \tag{4.24b}$$

First, results are shown in Figure 7 for the elliptic annulus without the use of interpolated points and $\bar{\mu}_1 = 1$ and $\bar{\mu}_2 = 1$. Here, D was chosen as the minimum thickness of the annulus. The pattern of results is similar to Figure 1. Next, we replot the error in Figure 8 as a function of $D/(\Delta S(1 - D|\kappa|/2))$, where the local Δs and κ are measured on the outer surface, and find that the error behavior is again well described by (4.15). Finally, in Figures 9 and 10, results are given when interpolated points are used, Fourier and cubic spline interpolation being used respectively.

The relative merits of using Fourier and cubic spline interpolation hinge upon accuracy versus cost. Our approach is to use a fixed number of quadrature points, hence the added cost is determined by the type of interpolation used. For illustrative purposes, we chose two disparate types of interpolation: discrete Fourier and periodic cubic splines. While the

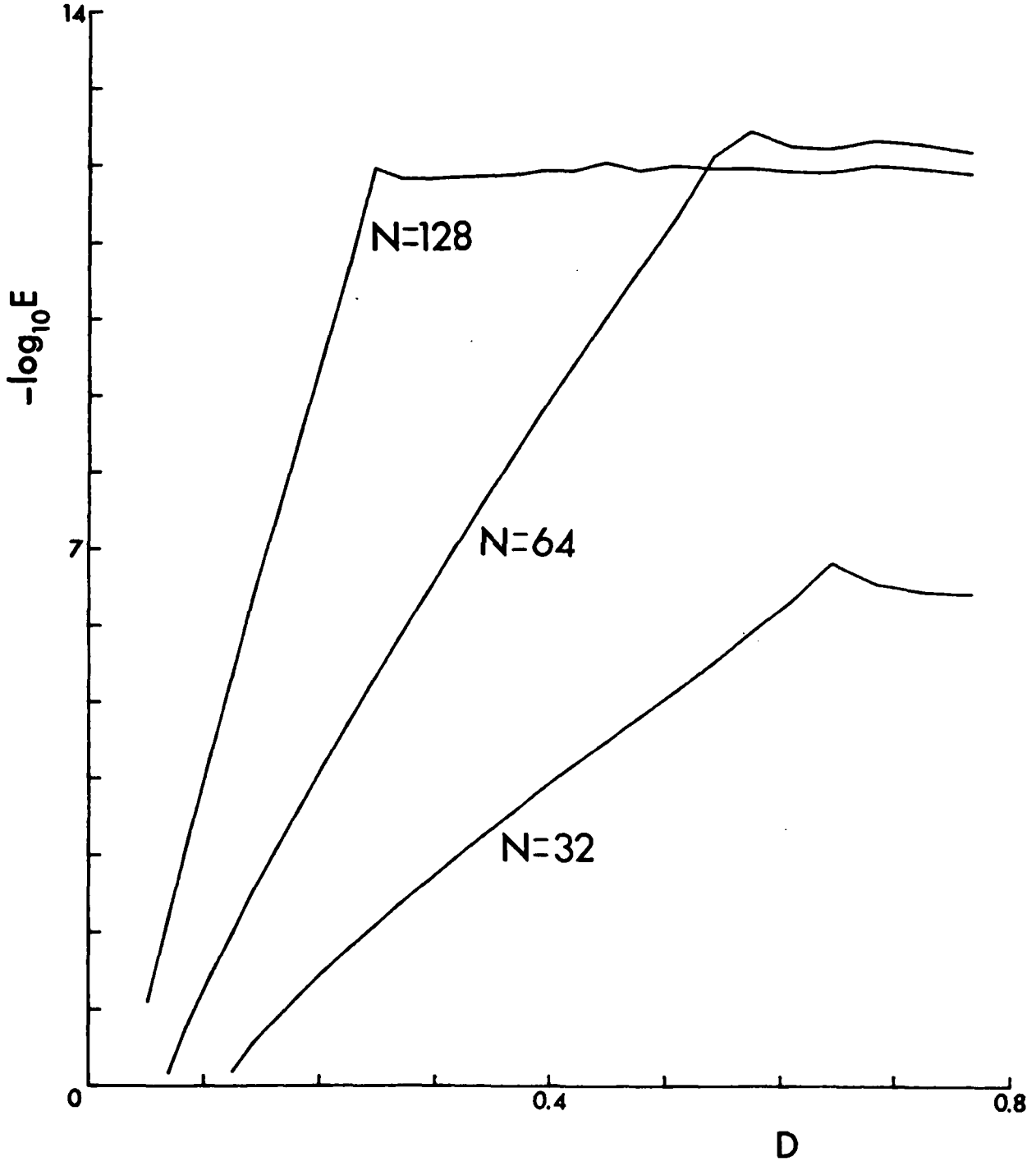

Figure 7. The maximum of the absolute error E in dpole sheet strength for the elliptic annulus as a function of D where D is the minimum thickness of the annulus.

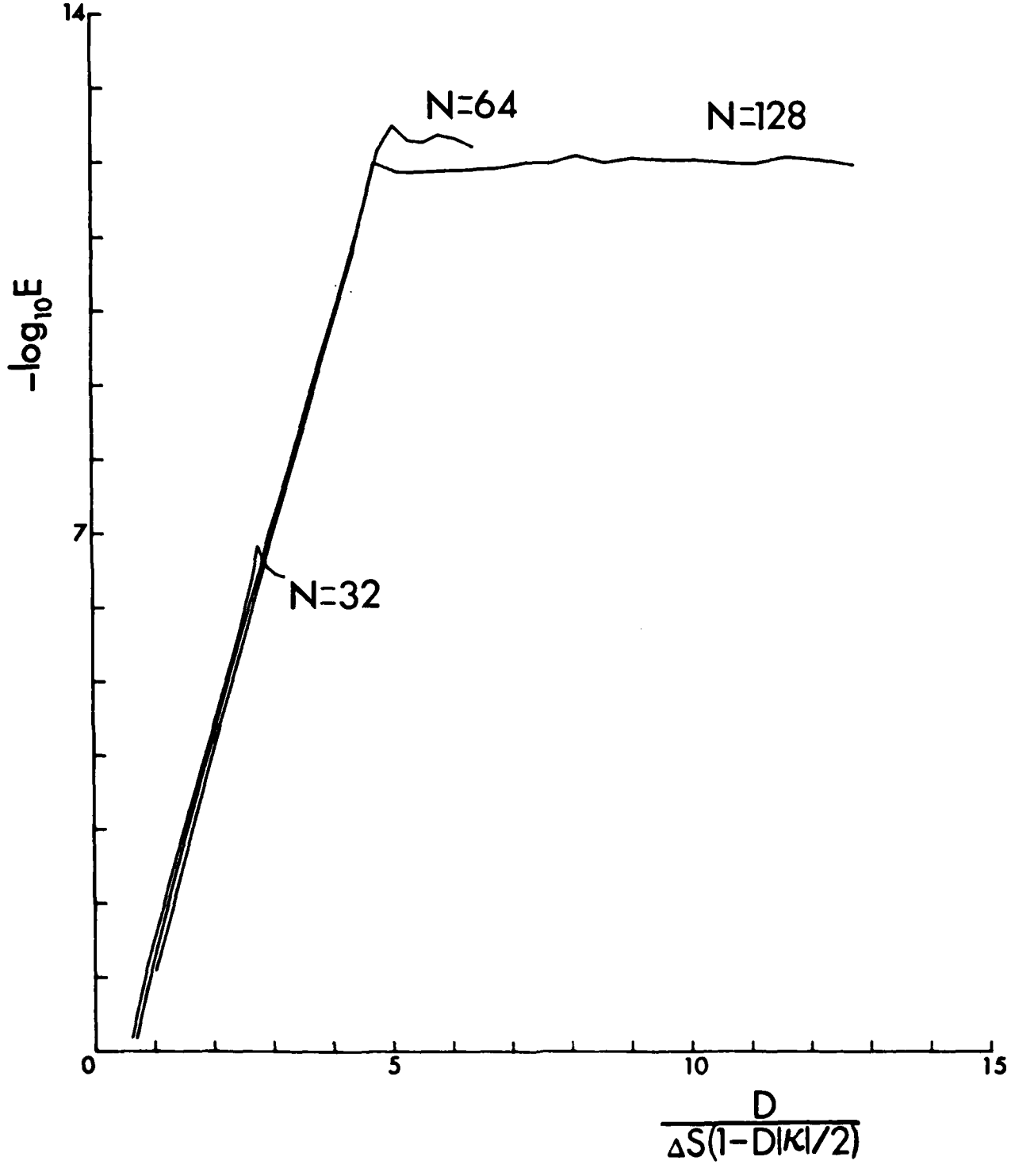

Figure 8. The same as Figure 7 except D is scaled by $\Delta S(1-D|\kappa|/2)$ where the local arclength between points, ΔS, and κ are measured on the outer boundary at the point of minimum thickness.

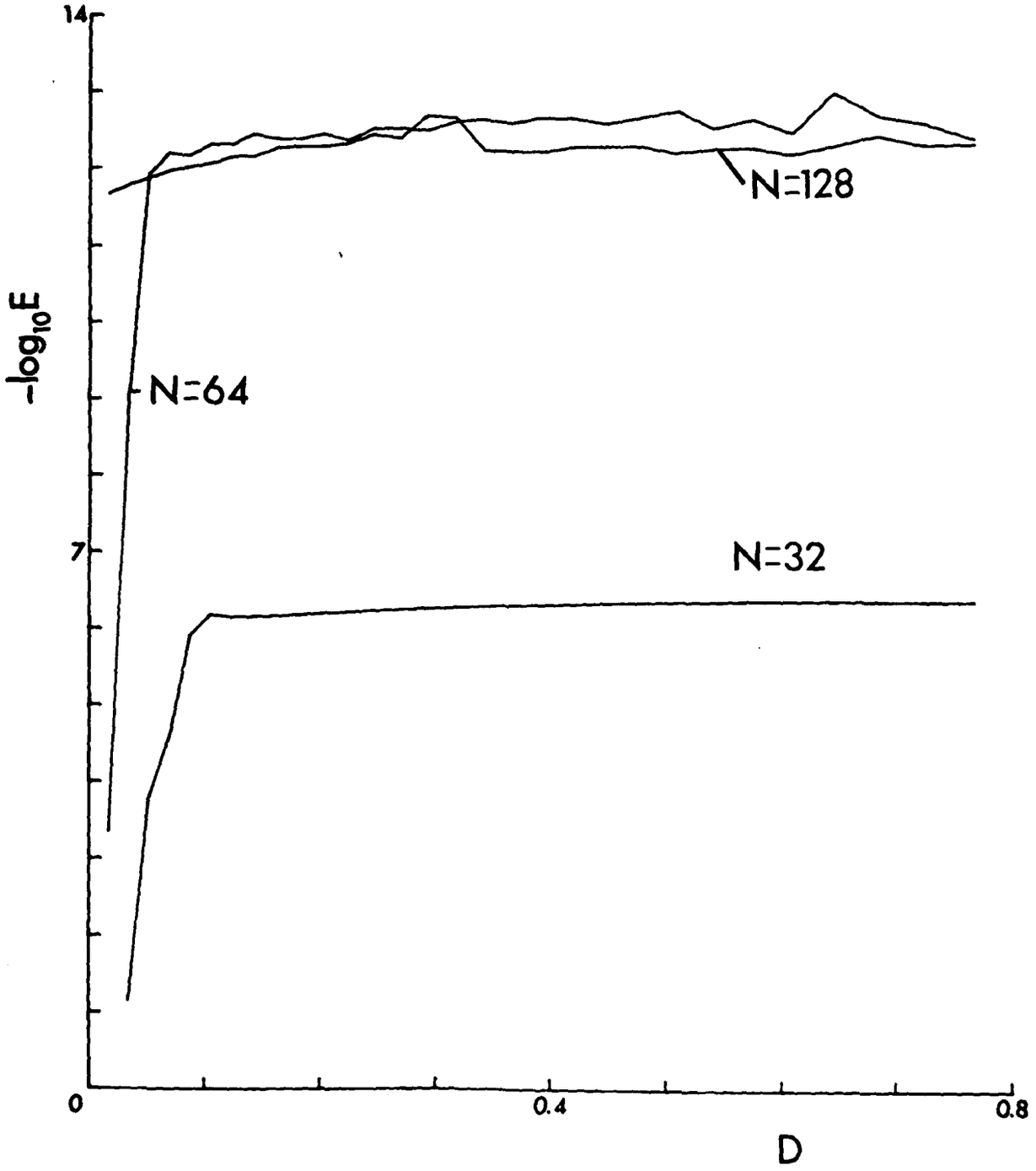

Figure 9. The maximum of the absolute error E in dipole sheet strength for the elliptic annulus as a function of D when Fourier interpolation is used to redistribute quadrature points.

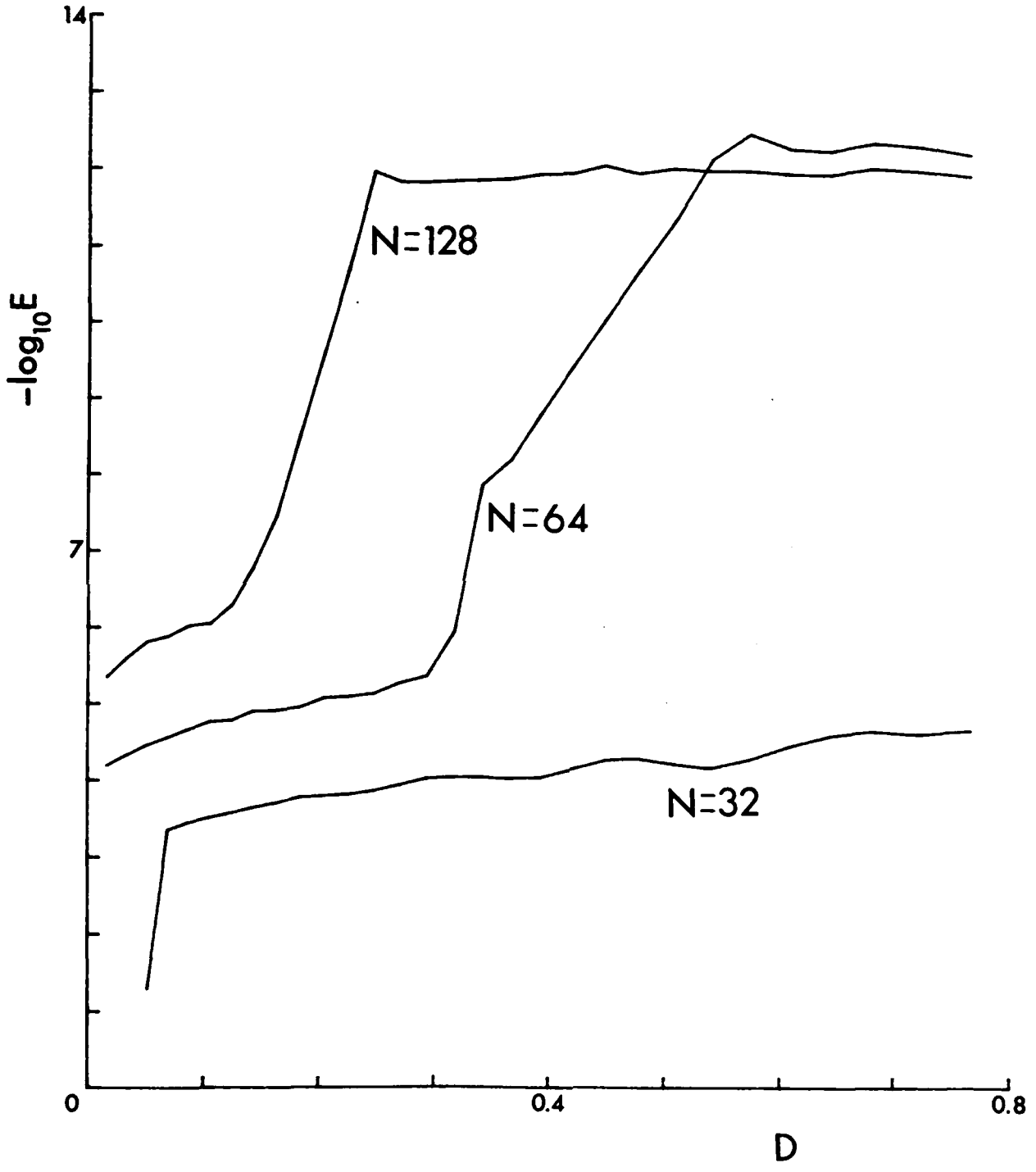

Figure 10. The same as Figure 9 except cubic spline interpolation is used.

Fourier interpolation is spectrally accurate, each interpolation involves a summation, and the cost is increased by a factor $O(N)$. Fortunately, Fourier interpolation is fully vectorizable, considerably reducing the cost. When the surface representation is "noisy", or the Fourier interpolation considered too expensive, periodic cubic splines offer an attractive alternative. The error is now at best $O(\Delta e^4)$, but the cost is only increased by a factor $O(1)$.

Section V. Conclusion

In conclusion, it is possible to solve elliptic problems in multi-connected domains with smooth boundaries using iterative boundary integral techniques. High accuracy is possible for relatively few boundary points, even when the multiconnected region has thin parts. A simple redistribution of points insures the high accuracy. This technique is now being applied to the study of accelerating, thin fluid shells (Baker 1983) and of the fluid motion of vortex layers; these results will be published elsewhere.

Acknowledgements.

We appreciate several useful discussions with D.I. Meiron.

References

1. G.R. Baker, (1983), in Waves on Fluid Interfaces. ed. Meyer, MRC, Wisconsin.

2. G.R. Baker, D.I. Meiron and S.A. Orszag, (1980). Phys. Fluids 23, p. 1485.

3. G.R. Baker, D.I. Meiron and S.A. Orszag, (1982). J. Fluid Mech. 123, p. 477.

4. S. C. Eisenstat, H. C. Elman and M. H. Schultz, (1983). SIAM J. Num. Anal. 20, p. 345

5. E. Isaacson and H.B. Keller, (1966). Analysis of Numerical Methods, Wiley.

6. M.A. Jaswon and G.T. Symm, (1977). Integral Equation Methods in Potential Theory and Elastostatics, Academic Press.

7. O.D. Kellogg, (1929). Foundations of Potential Theory, Dover.

8. M.S. Longuet-Higgins and E.D. Cokelet, (1976). Proc. R. Soc. Land. A350, 1.

9. B. Maskew, (1977). J. Aircraft 14, p. 188.

10. S.G. Mikhlin, (1957). Integral Equations, Pergamon.

11. D.I. Pullin (1982). J. Fluid Mech. 119, p. 507.

SECURITY CLASSIFICATION OF THIS PAGE (When Data Entered)

REPORT DOCUMENTATION PAGE

READ INSTRUCTIONS BEFORE COMPLETING FORM

1. REPORT NUMBER #2830	2. GOVT ACCESSION NO. AD-A158 171
3. RECIPIENT'S CATALOG NUMBER	
4. TITLE (and Subtitle) BOUNDARY INTEGRAL TECHNIQUES FOR MULTI-CONNECTED DOMAINS	5. TYPE OF REPORT & PERIOD COVERED Summary Report - no specific reporting period
	6. PERFORMING ORG. REPORT NUMBER
7. AUTHOR(s) G. R. Baker and M. J. Shelley	8. CONTRACT OR GRANT NUMBER(s) MCS-8302549 DAAG29-80-C-0041 NGT 03002800
9. PERFORMING ORGANIZATION NAME AND ADDRESS Mathematics Research Center, University of Wisconsin 610 Walnut Street Madison, Wisconsin 53706	10. PROGRAM ELEMENT, PROJECT, TASK AREA & WORK UNIT NUMBERS Work Unit Number 2 - Physical Mathematics
11. CONTROLLING OFFICE NAME AND ADDRESS (See Item 18 below)	12. REPORT DATE June 1985
	13. NUMBER OF PAGES 36
14. MONITORING AGENCY NAME & ADDRESS(if different from Controlling Office)	15. SECURITY CLASS. (of this report) UNCLASSIFIED
	15a. DECLASSIFICATION/DOWNGRADING SCHEDULE

16. DISTRIBUTION STATEMENT (of this Report)

Approved for public release; distribution unlimited.

17. DISTRIBUTION STATEMENT (of the abstract entered in Block 20, if different from Report)

18. SUPPLEMENTARY NOTES

U. S. Army Research Office
P. O. Box 12211
Research Triangle Park
North Carolina 27709

National Aeronautics & Space Administration
Washington, DC 20546

National Science Foundation
Washington, DC 20550

19. KEY WORDS (Continue on reverse side if necessary and identify by block number)

Boundary integral techniques, multi-connected domains, Fredholm integral equations

20. ABSTRACT (Continue on reverse side if necessary and identify by block number)

Several boundary integral techniques are available for the computation of the solution to Laplace's equation in multi-connected domains. However, for cases where the domain is changing, such as in incompressible, inviscid fluid flow with free surfaces, iterative methods are highly attractive. The paper describes one such formulation and tests it on circular and elliptic annuli. It is necessary to use interpolated quadrature points to maintain accuracy when regions of the annuli are thin.

DD FORM 1 JAN 73 1473 EDITION OF 1 NOV 65 IS OBSOLETE

UNCLASSIFIED

SECURITY CLASSIFICATION OF THIS PAGE (When Data Entered)

END

FILMED

10-85

DTIC